Published in final edited form as:
Integr Biol (Camb). 2011 January ; 3(1): 65–74. doi:10.1039/c0ib00058b.

Large-scale analysis of neurite growth dynamics on micropatterned substrates[†,‡]

Zachary D. Wissner-Gross[a,b], **Mark A. Scott**[b,c], **David Ku**[c], **Priya Ramaswamy**[c], and **Mehmet Fatih Yanik**[c,d,e]

[a]Department of Physics, Harvard University, 17 Oxford Street, Cambridge, MA 02138, USA

[b]Harvard-MIT Division of Health, Science, and Technology, 77 Massachusetts Avenue, Cambridge, MA 02139, USA

[c]Department of Electrical Engineering and Computer Science, Massachusetts Institute of Technology, 77 Massachusetts Avenue, Cambridge, MA 02139, USA

[d]Department of Biological Engineering, Massachusetts Institute of Technology, 77 Massachusetts Avenue, Cambridge, MA 02139, USA

[e]Massachusetts Institute of Technology, 77 Massachusetts Avenue, Room 36-834, Cambridge, MA 02139. yanik@mit.edu; Fax: 617-324-3534; Tel: 617-253-1583

Abstract

During both development and regeneration of the nervous system, neurons display complex growth dynamics, and several neurites compete to become the neuron's single axon. Numerous mathematical and biophysical models have been proposed to explain this competition, which remain experimentally unverified. Large-scale, precise, and repeatable measurements of neurite dynamics have been difficult to perform, since neurons have varying numbers of neurites, which themselves have complex morphologies. To overcome these challenges using a minimal number of primary neurons, we generated repeatable neuronal morphologies on a large scale using laser-patterned micron-wide stripes of adhesive proteins on an otherwise highly non-adherent substrate. By analyzing thousands of quantitative time-lapse measurements of highly reproducible neurite growth dynamics, we show that total neurite growth accelerates until neurons polarize, that immature neurites compete even at very short lengths, and that neuronal polarity exhibits a distinct transition as neurites grow. Proposed neurite growth models agree only partially with our experimental observations. We further show that simple yet specific modifications can significantly improve these models, but still do not fully predict the complex neurite growth behavior. Our high-content analysis puts significant and nontrivial constraints on possible mechanistic models of neurite growth and specification. The methodology presented here could also be employed in large-scale chemical and target-based screens on a variety of complex and subtle phenotypes for therapeutic discoveries using minimal numbers of primary neurons.

[†]Electronic supplementary information available: Fig. S1. Immunohistochemical staining of hippocampal neurons and their neurites. Fig. S2. Effect of vesicle trafficking rate on neuronal polarization in the Fivaz *et al.* model. See DOI: 10.1039/c0ib00058b

[‡]Author contributions: Z.W.G. and M.F.Y. designed research; Z.W.G., M.A.S., and P.R. built the apparatus; Z.W.G. performed research; Z.W.G. and D.K. analyzed data; and Z.W.G. and M.F.Y. wrote the paper.

Correspondence to: Mehmet Fatih Yanik.

Introduction

During development and regeneration, neurons undergo several complex morphological and functional changes, including neurite outgrowth, axon specification, branching, and synaptogenesis. Subtle abnormalities in these processes have been implicated in several neurological disorders such as autism,[1,2] schizophrenia,[3] and epilepsy.[4] Developing assays for repeatable recapitulation of these complex neuronal behaviors on a large scale could allow not only mechanistic studies but also large-scale high-content screens and therapeutic discoveries. However, due to the significant complexity and heterogeneity of neuronal dynamics, the development of such assays has proven challenging.

The dynamics of immature neurite growth and subsequent axon specification during development have been most extensively studied in primary hippocampal neurons from embryonic rats. Developing hippocampal neurons extend several immature neurites, one of which ultimately becomes the longer axon while the remaining neurites become the shorter dendrites,[5,6] *i.e.*, the neurons polarize. Axotomies of hippocampal neurons in culture have revealed that once one neurite grows 10–15 μm longer than the others, it usually becomes the axon.[7,8] The process of axon specification is believed to rely on feedback loops among the neurites, in which longer neurites promote their own growth and inhibit the growth of other neurites.[6,9] Several molecular components of these feedback loops have recently been identified.[10,11]

Previous studies of neurite growth have typically involved neurons growing freely on two-dimensional substrates[5,11–16] or along intersecting stripes.[17,18] However, measurements of reproducible neurite growth dynamics on these surfaces are difficult to perform because neurons have varying numbers of immature neurites, and because these neurites can grow in a wide variety of morphologies, allowing quantification of only simple aspects of neurite growth dynamics over many neurons. In addition, primary neurons are prohibitively difficult to isolate in large numbers, and they must also be cultured at a high cell density, thereby increasing the likelihood of cell-cell interactions and reducing the number of neurites that grow without contacting other cells.

Here, we circumvented these difficulties by using a simple strategy to generate highly reproducible neurite growth behavior in a high-throughput format. In recent years, numerous methods have been demonstrated that use surface patterning to guide neuron development.[13,17,19–28] However, surface patterning has never been previously used to perform high-content screens for elucidating neurite dynamics. Here, we used a femtosecond laser beam to pattern micron-wide lines of poly-$_{D}$-lysine (PDL) onto a poly(ethylene glycol) (PEG) monolayer (Fig. 1A and B). Hippocampal neurons preferentially adhered to the PDL lines, and the narrowness of these lines prevented each neuron from growing more than one neurite in each direction (Fig. 1C). By imaging the neurite growth dynamics of only about a hundred cells, we acquired thousands of data points with very high signal-to-noise ratio. In particular, we found that neurite growth accelerates until the point at which neurons polarize. We also showed that immature neurites compete, even at very short lengths, and that neuronal polarity exhibits a distinct phase transition as neurites grow.

A number of mathematically and biophysically inspired models of neurite outgrowth have been proposed in recent years.[9,11,29–36] In these models, small differences in neurite lengths and growth rates are amplified over time until one neurite becomes the axon, which continues to grow at a fairly constant rate, while all the other neurites become shorter dendrites or retract.[5] However, in the absence of large-scale quantitative experimental data, these different models have remained similarly plausible.

We selected three representative models, which we compared to our experimental findings. The simplest of these models describes neurite outgrowth as a competition for resources produced by the soma at a fixed rate and distributed to the different neurites as a function of their lengths.[29] More detailed biophysical models include the growth-dependent transport and diffusion of raw materials for neurite growth between the soma and the neurite tips.[30,31] Recently, a more complex and biochemically supported model was constructed based on a positive feedback loop between the GTPase HRas and phosphatidylinositol 3-kinase (PI3K) at the neurite tip.[11]

By finding the best fits of these models to our neurite growth data (*i.e.*, neurite length as a function of time), we first determined the unknown parameters used in these models. We then examined how well these models predicted neurite growth and competition dynamics. None of these models was fully consistent with our measurements. We found that although specific modifications of the complex molecular model of Fivaz *et al.*[11] allowed this model to better recapitulate our observations, these modified versions also did not completely agree with our results. Thus, such high-content measurements can put significant and nontrivial constraints on possible mechanistic models of neurite growth.

Results

Surface patterning

To create narrow protein stripes preventing growth of more than single neurites, an optical patterning technique was used with sub-micron resolution. Poly-D-lysine patterns were created using an improved version of laser-assisted protein adsorption by photobleaching (LAPAP).[37,38] The original LAPAP technique does not allow reliable growth of neurites along well-defined protein micropatterns, since cell bodies and neurites also grew on parts of the substrate that are not patterned. In order to overcome this challenge, rather than patterning onto a glass substrate coated with bovine serum albumin,[38] we developed a new method to pattern proteins onto a glass coated with a PEG monolayer (Fig. 1B). This significantly reduced non-specific cell adhesion and neurite growth, thereby allowing single neurites to grow on well-defined tracks and form highly repeatable morphological patterns. The glass was first cleaned with Nano-Strip (Cyantek) for 15 min, then rinsed in deionized water, air-dried, and placed in a toluene bath (Chromasolv Plus, Sigma). Subsequently, the bath was moved into a nitrogen bag, and PEG silane (2-[methoxy(polyethyleneoxy)propyl]trichlorosilane, Gelest) was added at a volumetric ratio of 2%. After 2 h, the bath was removed and the glass was rinsed in deionized water, air-dried, and placed in a vacuum oven for 2 h. Following removal from the vacuum oven, the glass was firmly attached to a silicone gasket of a 16-well plate (ProPlate slide module, Grace Bio-Labs).

We used a Ti : sapphire laser (Spectra-Physics) operating at 780 nm, near the two-photon absorption peak for fluorescein,[39] to pattern fluorescein dye (100 μg/ml, J. T. Baker) onto PEG-coated glass. Laser patterning was performed using a Nikon Eclipse Ti microscope equipped with a real-time focus correction system and a 40× objective lens (NA 0.9, Nikon). The laser power at the bottom surface of the glass slide was measured to be 7 mW, as estimated by multiplying the power level at the back focal-plane of the objective lens with its optical transmissivity. Patterns were created by scanning the laser beam at a speed of 200 μm/s using galvo mirrors (Cambridge Technology, UK) with a spatial resolution of 250 nm.

The PDL patterns consisted of 1 μm wide and 2 mm long lines with a line-to-line separation of 100 μm (Fig. 1A). After fluorescein patterning, each well of the 16-well plate was washed with phosphate buffered saline (PBS, Sigma) and then incubated for 1 min with PDL (10 μg/ml, 1–4 kDa, Sigma) fluorescently tagged with DyLight 549 (Pierce) to facilitate

visualization. The width of the lines was confirmed by fluorescent imaging. Variation in PDL concentration along individual lines was approximately 3%. Variation in average fluorescence between lines in the same well was also about 3%. Wells were washed again with PBS before cell plating.

Imaging and analysis

Rat hippocampal cells were isolated and plated as described in the methods. Neurons were imaged after plating using a CoolSnap HQ2 CCD camera. The motorized microscope stage (Prior ProScan) automatically scanned the sample to capture the entire patterned region. Immunohistochemical stains of tubulin confirmed that single neurites, rather than neurite bundles, grew out from the neurons along the PDL lines (Fig. S1).

We made a total of 3872 neurite length measurements, where individual neurons were imaged at 1-hour intervals for 18 h. The 18-hour time window was chosen because the competition between neurites vanished beyond this point as we show below. A representative measurement of a neuron is shown in Fig. 2A. On average, neurite growth in both directions along PDL lines was symmetric, with mean values of 33.2 ± 0.6 μm and 32.9 ± 0.5 μm (SEM, Fig. 2C), indicating that neurite outgrowth was not biased due to any anisotropy of the PDL patterns.

Growth velocity and acceleration were calculated for each of the neurites as a function of time. For a neurite with length $L(t)$, where t is the number of hours that have elapsed since the beginning of the observation, that neurite's velocity $\dot{L}(t)$ (in units of μm/h) was calculated using the relation $\dot{L}(t) = [L(t+1) - L(t-1)]/2$, and acceleration $\ddot{L}(t)$ (in units of $\mu m/h^2$) was calculated using $\ddot{L}(t) = L(t+1) - 2L(t) + L(t-1)$.

Parametric fitting of neurite growth models

Each neurite growth model we studied consists of several equations as well as parameters such as rate constants and diffusion/transport constants (Fig. 3), which were assumed to be the same for all neurons. Neurite lengths for the Khanin *et al.*[29] and Samuels *et al.*[30] models were calculated as a function of time using a fourth-order Runge–Kutta-Fehlberg differential equation solver (MATLAB function *ode*45), while a multistep stiff differential equation solver (MATLAB function *ode*15*s*) was used to calculate neurite lengths for the Fivaz *et al.* model.

Best-fit values for the unknown parameters as well as initial conditions were determined using an optimization scheme based on gradient descent, with additional constraints placed on the parameters as necessary, such as restricting values of physical quantities to be positive. Uncertainties in the estimation of these parameters were determined by randomly varying the initial conditions and the initial parameter values used in the optimization.

Importantly, the best-fit values of all unknown parameters were varied to assure that the general neurite growth behaviors (*i.e.*, neurite growth rate, competition, polarization) that we study in the following sections are not affected by the choice of these parameters.

The simplest model for neurite growth, proposed by Khanin *et al.* (Fig. 3A) predicts the specification of a single axon among several competing neurites.[29] The model assumes that the summation of the growth rate of all the neurites remains constant over time, and that the growth rate of an individual neurite increases with the neurite's length. We determined the two parameters of this model to be $v_0 = 7.2 \pm 0.4$ μm/h and $\alpha = 1.22 \pm 0.08$ (SEM), where v_0 is the characteristic growth rate, and the dimensionless α represents the strength of the competition between the neurites (Fig. 3A). This result falls within the regime where axon specification occurs ($\alpha > 1$).[29]

Samuels *et al.* proposed a model of intermediate complexity (Fig. 3B), consisting of five coupled differential equations in the case of two competing neurites.[30] A sample fitting of this model to neurite data is shown in Fig. 2B. The model was based on the diffusive and active transport of a rate-limiting factor for neurite growth, although the identity of this factor was unknown. Similar models have proposed that this rate-limiting material is tubulin.[31,35] The Samuels model consists of six parameters: three dimensionless constants (χ_1, χ_2, and χ_3), and a characteristic length (L_{sc}), time (t_{sc}), and concentration (C_{sc}). We reduced the number of these parameters to five by normalizing concentrations C_0, C_1, and C_2 with respect to C_{sc}. The measured values for the parameters were t_{sc}=6.4 ± 0.5 h, L_{sc} = 51.3 ± 4.6 μm, χ_1 = 5.7 ± 0.9, χ_2 = 36.8 ± 3.8, and χ_3 = 5.2 ± 1.3. These values for χ_1 and χ_2 fall within the regime where axon specification occurs.[30]

The third model we compared to our data was proposed by Fivaz *et al.*, who identified a positive feedback loop between HRas and PI3K at the neurite tip as the primary recruiter of additional HRas to the neurite tip and as a driving mechanism for neurite growth and competition.[11] We used similar values for all parameters to those suggested by the authors, as these already produced good fits to the measured neurite lengths as a function of time.[11]

Analysis of neurite growth dynamics

To quantify neurite growth behavior, we first analyzed *total neurite growth rate* to see whether total growth remained constant or was accelerative, since different neurite growth models make different predictions on this point. As the neurites grow, they also compete against each other. Thus, *neurite competition* was the second metric used in our analysis. Finally, we studied the overall *neuronal polarity*, which we expected to become more observable as one neurite out-competed the other.

1. Total neurite growth rate—We observed that the total neurite growth rate increased with total neurite length, *i.e.*, total neurite growth was accelerative (Fig. 4A), up to a length of approximately 80 μm. This acceleration was fastest when both neurites were very short, although there was greater uncertainty associated with these measurements.

To determine whether the models predicted this accelerative growth, initial neurite lengths were randomized between 1 and 5 μm based on our experimental observations. The initial normalized concentrations (C_0, C_1, C_2) in the soma and neurite tips in the Samuels *et al.* model were randomized between 0 and 0.5 *i.e.*, within the range of values produced by parametric fitting. The initial chemical concentrations (*i.e.*, S, P_1, P_2, T_1, T_2, D_1, D_2) in the Fivaz *et al.* model were randomized between 0 and twice their respective equilibrium concentrations.

The Khanin *et al.* model predicts that the total neurite growth rate is constant and independent of total neurite length, and that there is no acceleration of total neurite growth (Fig. 4B).[29] Thus, the Khanin *et al.* model is not consistent with our total neurite growth measurements.

Meanwhile, the Samuels *et al.* model, predicts that the total growth rate of neurons with short neurites rapidly increases (Fig. 4C). This prediction is consistent with our experimental results.

For the Fivaz *et al.* model, the acceleration of total neurite growth does not agree with our experimental data (Fig. 4D). Indeed, a sustained increase in growth rate is not possible in the Fivaz *et al.* model because the total amount of the growth-inducing factor HRas within each neuron is fixed by the initial conditions.

We then made several simple modifications to the Fivaz *et al.* model, since this model has a well supported molecular basis.[11] These modifications were made independently of each other and were each capable of recapitulating accelerative total neurite growth (although their effects on other characteristics of neurite growth dynamics, which we discuss next, were significantly different). The first modification introduced a nuclear source term for HRas that declines as neuron matures (Fig. 4E), since the total neurite growth rate depends on the total amount of available HRas in the neuron. A second modification introduced a nuclear source term for PIP_2, which could then be phosphorylated into PIP_3 by PI3K at the neurite tip (Fig. 4F), as the neurite growth rates are proportional to the concentrations of PIP_3 in the neurite tips. The third modification increased the rate of vesicle trafficking of HRas as the neurons developed ("dynamic trafficking" in Fig. 4G), since increasing the rate of HRas trafficking should also increase the total neurite growth rate. These modifications to the Fivaz *et al.* model are further detailed in the methods section.

2. Neurite competition—Neurite growth rates depend on the concentrations of growth-limiting factors in the neurite tips.[11,30,31] Neurites compete for these factors to increase their length,[6] and neurite growth rate, $\dot{L}$, reflects the concentrations of these factors. To quantify the dynamics of this competition (*i.e.* changes in concentrations of growth-limiting factors), we therefore evaluated correlations in the changes in neurite growth rates (*i.e.*, acceleration, $\ddot{L}$). We define the neurite competition factor (NCF) between two neurites as the normalized product of their accelerations:

$$\mathrm{NCF} = -\frac{\ddot{L}_1 \ddot{L}_2}{|\ddot{L}_1| + |\ddot{L}_2|} \tag{1}$$

A positive NCF corresponds to competitive behavior between the neurites, while a negative NCF corresponds to cooperative behavior, as shown in Fig. 5.

We experimentally observed that as one neurite's growth rate increased, the growth rate of the other neurite on average always decreased (*i.e.*, positive NCF in Fig. 4H for all neurite lengths). The relative growth rates of neurites often alternated, such that both neurites grew to substantial lengths. We observed this competitive behavior over a range of neurite lengths, even when the total neurite lengths were as short as 20 μm and as long as 100 μm. This competition was strongest when the total neurite length was between 50 and 60 μm.

We next evaluated how well the different models predicted the observed competition between growing neurites. The Khanin *et al.* model predicts that the growth rate of one of the two neurites will be always increasing while the other is always decreasing. As a result, the model incorrectly predicts that the competition between neurites starts highest and monotonically decreases as neurites grow (Fig. 4I). This prediction is inherent to the Khanin *et al.* model, and does not depend on the choice of parameters v_0 and α.

The Samuels *et al.* model also diverges significantly from the experimentally observed competitive behavior for shorter total neurite lengths (<50 μm) (Fig. 4J). The model inherently and incorrectly predicts that the growth rates of both neurites increase (negative NCF in Fig. 4J) until

$$\frac{L_i}{L_{sc}} > \frac{\chi_1 (C_i - C_0)}{C_i (\chi_2 C_0 - 1)} \sim \frac{2\chi_1}{\chi_2} \tag{2}$$

where L_i is the length of the shorter neurite, and C_i is the corresponding resource concentration at that neurite's tip. The factor of 2 in the above relation was determined

empirically from typical concentrations produced by our fitting analysis. The numerator and denominator on the right-hand side of eqn (2) are respectively proportional to the diffusion and active transport rates of the resource. When L_i/L_{sc} is larger than the ratio of the two rates (*i.e.* diffusion is slower than active transport), the growth rate of the shorter neurite will begin to decrease, *i.e.*, NCF becomes positive. This transition in NCF occurs when L_i is approximately 15 μm, which implies a total neurite length of at least 30 μm, *i.e.*, twice the length of the shorter neurite. This was in agreement with our numerical simulations of the model (Fig. 6J). However, it was inconsistent with our experimental data, in which NCF was positive even at total neurite lengths much shorter than 30 μm.

We found that the Fivaz *et al.* model correctly predicted competition between the neurites, even at shorter neurite lengths (*i.e.*, positive NCF in Fig. 4 K). Our modifications of the model also predicted competition correctly at shorter neurite lengths (Fig. 4L-N), although the addition of a PIP source term appeared to result in an NCF that increased monotonically with neurite length (Fig. 4M). The addition of dynamic trafficking resulted in the strongest competitive trend and a maximal NCF closest to what we observed experimentally. However, the original Fivaz *et al.* model and all modifications of the model predicted a significantly positive NCF even at longer neurite lengths, inconsistent with our experimental observations.

3. Neuronal polarization—Neurons polarize as their neurites grow, as discussed in the introduction, and such polarization was evident in our experiments as total neurite length exceeded 80 μm (Fig. 4O). Here, we define neuronal polarity as $|L_1-L_2|/(L_1+L_2)$. The increase in polarity occurred quite suddenly and is suggestive of a phase transition, which occurs in various biological phenomena.[40,41]

The polarization process predicted by the different neurite growth models demonstrated a variety of behaviors. For comparison, we set the initial neurite lengths in all the models to be the same to match the initial mean polarity (~0.2) we measured experimentally.

No phase transition was evident in the Khanin *et al.* model, which produced a polarity that steadily increased with total neurite length (Fig. 4P). Polarity in the Samuels *et al.* model more closely resembled our experimental results (Fig. 4Q). Like the Khanin *et al.* model, the Fivaz *et al.* model produced an increasing polarity (Fig. 4R) inconsistent with our experiments.

Our modifications of the Fivaz *et al.* model also resulted in distinct polarity behaviors. Introduction of an HRas source term caused the neuron to polarize at shorter lengths (Fig. 4S), while the PIP source term appeared to lower the steady-state neuronal polarity (Fig. 4T). These were inconsistent with the polarization behavior we measured. Our experimental observations were best predicted by the dynamic vesicle-trafficking modification, which resulted in a nearly constant polarity of about 0.2 for total lengths under 100 μm, and an increasing polarity for lengths exceeding 100 μm (Fig. 4U). This apparent phase transition occurs when the vesicular trafficking rate exceeds a critical value of 0.6 vesicles/min (Fig. S2).

Discussion

Large-scale studies of neurite dynamics have remained difficult to perform because neurites branch and grow in various morphologies. By growing neurons on protein micropatterns, we dramatically increased the repeatability of neurite growth behavior. This enabled us to measure and analyze the dynamics of neurite growth acceleration, neurite competition, and

neuronal polarity with unprecedented reproducibility using a minimal number of primary neurons.

We specifically found that neurites compete with each other, even when total neurite length is as short as 20 μm. This is a non-obvious behavior, as certain models predict incorrectly that both neurites can accelerate simultaneously. We also found that total neurite growth is also accelerating at these shorter lengths. Then, as total neurite length increases beyond a critical length (~80 μm in our assays), several events occur simultaneously: the neuron polarizes (Fig. 4O), total neurite acceleration approaches zero while the total neurite growth rate reaches a steady-state value (Fig. 4A), and neurite competition ceases (Fig. 4H).

We were further able to evaluate several leading models of neurite growth by analyzing their ability to predict these fundamental biophysical behaviors of neurite growth and axon specification (Table 1). The Khanin *et al.* model was empirically hypothesized and is incapable of reproducing behaviors similar to our experimental observations, since it presumes a constant total growth rate. The model therefore exhibits zero total neurite acceleration (Fig. 4B). In addition, the model incorrectly predicts that the strongest competition (*i.e.*, the highest NCF) occurs while neurites are shortest and that neuronal polarity smoothly increases with total neurite length (Fig. 4P).

Unlike the Khanin *et al.* model, the Samuels *et al.* model proposes a chemical mechanism for neurite growth. In this model, growth depends on the concentration of a specific chemical that is actively transported from the soma to the neurite tips, that passively diffuses between these locations, and that is consumed during neurite growth. At shorter lengths, diffusion between neurites occurs rapidly, allowing the neurites to effectively share a common pool of resources when they are short. As a result, short neurites grow cooperatively until reaching lengths at which active transport begins to dominate (see Fig. 4Q and eqn (2)). Thus, while this model correctly predicts accelerative total neurite growth (Fig. 4C), it results in cooperative rather than competitive behavior for neurites shorter than the length at which the active transport rate exceeds diffusion.

The Fivaz *et al.* model includes the transport of several chemicals known to be involved in the establishment of neuronal polarity, allowing it to exhibit more complex behaviors than those of the Samuels *et al.* model. While the Fivaz *et al.* model correctly predicts that both shorter and intermediate neurites compete, the model does not predict accelerative growth at short neurite lengths (Fig. 4D), since the total amount of HRas (necessary for neurite growth) is fixed in the model. By including source terms for HRas and PIP, we were able to recapitulate accelerative growth in this model (Fig. 4E and F). However, neither these modifications nor the original model predicts the sharp phase transition that occurs during neuronal polarization (Fig. 4R-T), suggesting that some additional mechanism is missing in this model. We hypothesized that a stronger nonlinearity between neurite length and neurite growth is necessary to induce such a sharp transition in polarity. As an example, we introduced such a nonlinear mechanism in the form of a time-dependent vesicle trafficking because neuronal polarization strongly depends on vesicle trafficking rate (Fig. S2). This modification successfully recapitulated the observed phase transition in polarity. We note that other nonlinear mechanisms are also plausable that could recapitulate such a sharp phase transition in polarity, and further biochemical assays are necessary to identify the nature of this nonlinear mechanism. Although our modifications significantly improved agreement of the Fivaz *et al.* model with our measurements, there were still minor but measurable differences (*e.g.*, none of the modifications recapitulated the weaker competition between long neurites). Thus, our high-content measurements put significant and nontrivial constraints on possible mechanistic models of neurite growth that cannot be reconciled by simple modifications. While biochemical assays in the future will be necessary to validate

any model, quantification of neurite dynamics by our technique allows discrimination of different mechanistic models.

It is possible that restricting neuronal adhesion and neurite growth to one dimension affects neurite competition and axon specification. However, we still observe all of the neurite growth and competition dynamics previously measured with standard two-dimensional cell culture techniques. Further-more, the mechanistic models we evaluated allow for any number of neurites, including two, and do not depend on the relative orientations of neurites. Thus, it is likely that the highly repeatable neurite dynamics we observe here extend to more complex morphologies of developing neurons.

This work represents the most quantitative description of neurite growth and competition to date. The protein patterning and analytical strategies developed here can be extended to analyze more complex neurite dynamics. These high-content measurement techniques can allow construction and validation of models for complex neuronal processes. They could also be used for large-scale chemical and target-based screens on a variety of complex phenotypes for therapeutic discoveries using a minimal number of primary neurons.

Methods

Cell culture and plating

Hippocampi were dissected from embryonic day 18 Sprague-Dawley rats and placed in ice-cold Hank's balanced salt solution (HBSS), buffered with 10 mM HEPES, pH 7.3. The tissue was transferred to an enzyme solution containing 100 units of papain in 5 ml of HBSS, 1 mM $CaCl_2$, and 1 mM L-cystine, and subsequently incubated at 37 °C for 45 min. The hippocampi were then washed in Dulbecco's modified Eagle's medium containing 10% fetal bovine serum to deactivate the papain, and the media was replaced with Neurobasal-B27 (Invitrogen) containing 2 mM glutamine and 100 units/ml penicillin/streptomycin. The cells were triturated using a flame-polished pipette and counted.

200 ml of Neurobasal-B27 were added to each well containing the PDL patterns. Cells were then pipetted into the wells at a density of 5000 cells per well. The cells were maintained in an incubator at 37 °C with 5% CO_2 and 100% humidity, and were briefly removed every hour for imaging.

Immunohistochemistry

Cells plated on PDL patterns for 12 h were fixed for 15 min in 4% paraformaldehyde and then rinsed with a solution of phosphate buffered saline with 0.05% Tween 20 (PBST). Next, the cells were permeabilized with 0.1% Triton X-100 for 10 min, and washed again with PBST.

Prior to antibody staining, the surface was blocked with 3% bovine serum albumin for 30 min. Cells were incubated in a 1 : 1000 dilution of mouse monoclonal anti-tubulin (primary antibody, R&D Systems) for 1 h, and then in a 1 : 500 dilution of Alexa Fluor 488 goat anti-mouse (secondary antibody, Invitrogen) for another hour, with PBST washing between steps. Finally, the cells were incubated in a 1 : 10 000 dilution of DAPI for nuclear staining, washed again, and fluorescently imaged.

Modifications to the Fivaz *et al.* model

The original model proposed by Fivaz *et al.* consisted of the equations shown in Fig. 3C, which are rewritten here with the stochastic anterograde vesicular trafficking terms $V_i(t)$ included:

$$\dot{P}_i = \frac{k_P(T_i + R_b)}{K_M + T_i + R_b} - \varphi P_i$$
$$\dot{T}_i = k_{R1} D_i (P_i + P_b) - (\rho + \beta) T_i$$
$$\dot{D}_i = k_{R0} S (P_i V_i(t) + P_b) - \beta D_i + \rho T_i - k_{R1} D_i (P_i + P_b)$$
$$\dot{S} = \beta (D_1 + D_2 + T_1 + T_2) - k_{R0} S (P_1 V_1(t) + P_2 V_2(t) + 2P_b)$$
$$\dot{L}_i = k_L (P_i + P_b).$$

Fivaz *et al.* defined $V_i(t)$ as follows:

$$V_i(t) = \frac{1}{\sigma \sqrt{2\pi}} \sum_f \exp\left(-\frac{(t - t_f)}{2\sigma^2}\right),$$

where vesicles containing HRas release their contents at the neurite tip at times t_f and σ is the temporal width of the HRas release by the vesicles. Like Fivaz *et al.*, here we assume an average vesicle trafficking rate of 1 vesicle per minute for each neurite.

Our first modification of the model was to include a term representing the nuclear synthesis of HRas that declines as the neuron matures. This was accomplished by adding a decaying source term to the equation for *S*:

$$\dot{S} = \gamma \exp\left(-\frac{L_1 + L_2}{\lambda}\right) + \beta (D_1 + D_2 + T_1 + T_2) - k_{R0} S (P_1 V_1(t) + P_2 V_2(t) + 2P_b),$$

where the characteristic length λ was set to 50 μm. The magnitude γ of the source term was varied in Fig. 4.

The second modification was the introduction of a PIP_2 source term in neurites that also declines as the neuron matures. We define Q_i as the concentration of PIP_2 in neurite *i*. The equation for *P* is then

$$\dot{P}_i = \frac{k_P(T_i + R_b)}{K_M + T_i + R_b} Q_i - \varphi P_i,$$

and we introduce a similar equation for *Q*:

$$\dot{Q} = \kappa \exp\left(-\frac{L_1 + L_2}{\lambda}\right) + \varphi P_i - \frac{k_P(T_i + R_b)}{K_M + T_i + R_b} Q_i.$$

Again, λ was set to 50 μm, and the magnitude κ of the source term was varied in Fig. 4.

The third modification (“dynamic trafficking”) added time dependence to the vesicle trafficking rate. This rate was initially set to zero, and exponentially approached a steady-state value of 1 vesicle per minute per neurite with a characteristic time τ, which was varied in Fig. 4.

Insight, innovation, integration

A number of models have been proposed in recent years to explain how neurites of developing and regenerating neurons grow and compete with each other. However, none of these models has been validated due to significant challenges in measuring neurite growth dynamics with sufficient repeatability to extract the fine dynamics of neurite

growth. Using a novel analysis and protein patterning technique that restricts the growth of individual neurites on a substrate that otherwise prevents adhesion of neurons and neurites, we elicited and quantified several important yet previously unknown aspects of neurite competition and neuronal polarity. Our high-content analysis puts significant and nontrivial constraints on possible mechanistic models of neurite growth.

Supplementary Material

Refer to Web version on PubMed Central for supplementary material.

Acknowledgments

ZWG thanks A. D. Wissner-Gross for helpful discussions regarding the analyses and manuscript. ZWG was supported by the Department of Defense (DoD) through the National Defense Science & Engineering Graduate (NDSEG) Fellowship Program and by a Fannie and John Hertz Foundation/Myhrvold Family fellowship. MAS was supported by the Kennedy Memorial Trust. MFY was supported by a Packard Fellowship in Science and Engineering and an Alfred Sloan Award. This project was funded by NIH Director's New Innovator Award (1-DP2-OD002989-01), part of the NIH Roadmap for Medical Research, and by NIH R01 EUREKA Award (1-R01-NS066352-01).

References

1. Südhof TC. Neuroligins and neurexins link synaptic function to cognitive disease. Nature. 2008; 455:903–911. [PubMed: 18923512]
2. Geschwind DH, Levitt P. Autism spectrum disorders: developmental disconnection syndromes. Curr. Opin. Neurobiol. 2007; 17:103–111. [PubMed: 17275283]
3. Bellon A. New genes associated with schizophrenia in neurite formation: a review of cell culture experiments. Mol. Psychiatry. 2007; 12:620–629. [PubMed: 17440437]
4. Larner AJ. Axonal sprouting and synaptogenesis in temporal lobe epilepsy: possible pathogenetic and therapeutic roles of neurite growth inhibitory factors. Seizure. 1995; 4:249–258. [PubMed: 8719916]
5. Dotti CG, Sullivan CA, Banker GA. The establishment of polarity by hippocampal neurons in culture. J. Neurosci. 1988; 8(4):1454–1458. [PubMed: 3282038]
6. Arimura N, Kaibuchi K. Neuron polarity: from extracellular signals to intracellular mechanisms. Nat. Rev. Neurosci. 2007; 8:194–205. [PubMed: 17311006]
7. Dotti CG, Banker GA. Experimentally induced alteration in the polarity of developing neurons. Nature. 1987; 330:254–256. [PubMed: 3313064]
8. Goslin K, Banker G. Experimental observations on the development of polarity by hippocampal neurons in culture. J. Cell Biol. 1989; 108:1507–1516. [PubMed: 2925793]
9. Andersen SSL, Bi G-q. Axon formation: a molecular model for the generation of neuronal polarity. BioEssays. 2000; 22:172–179. [PubMed: 10655036]
10. Menager C, Arimura N, Fukata Y, Kaibuchi K. PIP3 is involved in neuronal polarization and axon formation. J. Neurochem. 2004; 89:109–118. [PubMed: 15030394]
11. Fivaz M, Bandara S, Inoue T, Meyer T. Robust neuronal symmetry breaking by Ras-triggered local positive feedback. Curr. Biol. 2008; 18:44–50. [PubMed: 18158244]
12. Lamoureux P, Buxbaum RE, Heidemann SR. Axonal outgrowth of cultured neurons in not limited by growth cone competition. J. Cell. Sci. 1998; 111:3245–3252. [PubMed: 9763518]
13. Esch T, Lemmon V, Banker G. Local presentation of substrate molecules directs axon specification by cultured hippocampal neurons. J. Neurosci. 1999; 19(15):6417–6426. [PubMed: 10414970]
14. Diefenbach TJ, Guthrie PB, Kater SB. Stimulus history alters behavioral responses of neuronal growth cones. J. Neurosci. 2000; 20(4):1484–1494. [PubMed: 10662838]
15. Yu LMY, Wosnick JH, Shoichet MS. Miniaturized system of neurotrophin patterning for guided regeneration. J. Neurosci. Methods. 2008; 171:253–263. [PubMed: 18486231]

16. Zheng JQ. Turning of nerve growth cones induced by localized increases in intracellular calcium ions. Nature. 2000; 403:89–93. [PubMed: 10638759]
17. Withers GS, James CD, Kingman CE, Craighead HG, Banker GA. Effects of substrate geometry on growth cone behavior and axon branching. J. Neurobiol. 2006; 66:1183–1194. [PubMed: 16858695]
18. Oliva AA, James CD, Kingman CE, Craighead HG, Banker GA. Patterning axonal guidance molecules using a novel strategy for microcontact printing. Neurochem. Res. 2003; 28(11):1639–1648. [PubMed: 14584818]
19. Wheeler BC, Corey JM, Brewer GJ, Branch DW. Microcontact printing for precise control of nerve cell growth in culture. J. Biomech. Eng. 1999; 121:73–78. [PubMed: 10080092]
20. Luo Y, Shoichet MS. A photolabile hydrogel for guided three-dimensional cell growth and migration. Nat. Mater. 2004; 3:249–253. [PubMed: 15034559]
21. Welle A, Horn S, Schimmelpfeng J, Kalka D. Photo-chemically patterned polymer surfaces for controlled PC-12 adhesion and neurite guidance. J. Neurosci. Methods. 2005; 142:243–250. [PubMed: 15698664]
22. Li GN, Liu J, Hoffman-Kim D. Multi-molecular gradients of permissive and inhibitory cues direct neurite outgrowth. Ann. Biomed. Eng. 2008; 36(6):889–904. [PubMed: 18392680]
23. Dertinger SKW, Jiang X, Li Z, Murthy VN, Whitesides GM. Gradients of substrate-bound laminin orient axonal specification of neurons. Proc. Natl. Acad. Sci. U. S. A. 2002; 99(20):12542–12547. [PubMed: 12237407]
24. Rosoff WJ, et al. A new chemotaxis assay shows the extreme sensitivity of axons to molecular gradients. Nat. Neurosci. 2004; 7(6):678–682. [PubMed: 15162167]
25. Shi P, Shen K, Kam LC. Local presentation of L1 and N-cadherin in multicomponent, microscale patterns differentially direct neuron function *in vitro*. Dev. Neurobiol. 2007; 67(13):1765–1776. [PubMed: 17659593]
26. Clark P, Britland S, Connolly P. Growth cone guidance and neuron morphology on micropatterned laminin surfaces. J. Cell Sci. 1993; 105:203–212. [PubMed: 8360274]
27. Kaehr B, Allen R, Javier DJ, Currie J, Shear JB. Guiding neuronal development with *in situ* microfabrication. Proc. Natl. Acad. Sci. U. S. A. 2004; 101(46):16104–16108. [PubMed: 15534228]
28. Philipsborn, ACv, et al. Microcontact printing of axon guidance molecules for generation of graded patterns. Nat. Protoc. 2006; 1(3):1322–1328. [PubMed: 17406418]
29. Khanin K, Khanin R. A probabilistic model for establishment of neuron polarity. J. Math. Biol. 2001; 42(1):26–40. [PubMed: 11271507]
30. Samuels DC, Hentschel HGE, Fine A. The origin of neuronal polarization: a model of axon formation. Philos. Trans. R. Soc. London, Ser. B. 1996; 351:1147–1156. [PubMed: 8899865]
31. Veen MPV, Van Pelt J. Neuritic growth rate described by modeling microtubule dynamics. Bull. Math. Biol. 1994; 56(2):249–273. [PubMed: 8186754]
32. Tsaneva-Atanasova K, Burgo A, Galli T, Holcman D. Quantifying neurite growth mediated by interactions among secretory vesicles, microtubules, and actin networks. Biophys. J. 2009; 96:840–857. [PubMed: 19186125]
33. Li G-H, Qin C-D. A model for neurite growth and neuronal morphogenesis. Math. Biosci. 1996; 132:97–110. [PubMed: 8924723]
34. McLean DR, Graham BP. Stability in a mathematical model of neurite elongation. Math. Med. Biol. 2006; 23:101–117. [PubMed: 16672287]
35. Ooyen, Av; Graham, BP.; Ramakers, GJA. Competition for tubulin between growing neurites during development. Neurocomputing. 2001; 38–40:73–78.
36. McLean DR, Graham BP. Mathematical formulation and analysis of a continuum model for tubulin-driven neurite elongation. Proc. R. Soc. London, Ser. A. 2004; 460(2048):2437–2456.
37. Holden MA, Cremer PS. Light activated patterning of dye-labeled molecules on surfaces. J. Am. Chem. Soc. 2003; 125:8074–8075. [PubMed: 12837056]

38. Belisle JM, Correia JP, Wiseman PW, Kennedy TE, Costantino S. Patterning protein concentration using laser-assisted adsorption by photobleaching, LAPAP. Lab Chip. 2008; 8:2164–2167. [PubMed: 19023482]

39. Xu C, Webb WW. Measurement of two-photon excitation cross sections of molecular fluorophores with data from 690 to 1050 nm. J. Opt. Soc. Am. B. 1996; 13(3):481–491.

40. Berg HC, Brown DA. Chemotaxis in *Escherichia coli* analysed by three-dimensional tracking. Nature. 1972; 239:500–504. [PubMed: 4563019]

41. Mitchison T, Kirschner M. Dynamic instability of microtubule growth. Nature. 1984; 312:237–242. [PubMed: 6504138]

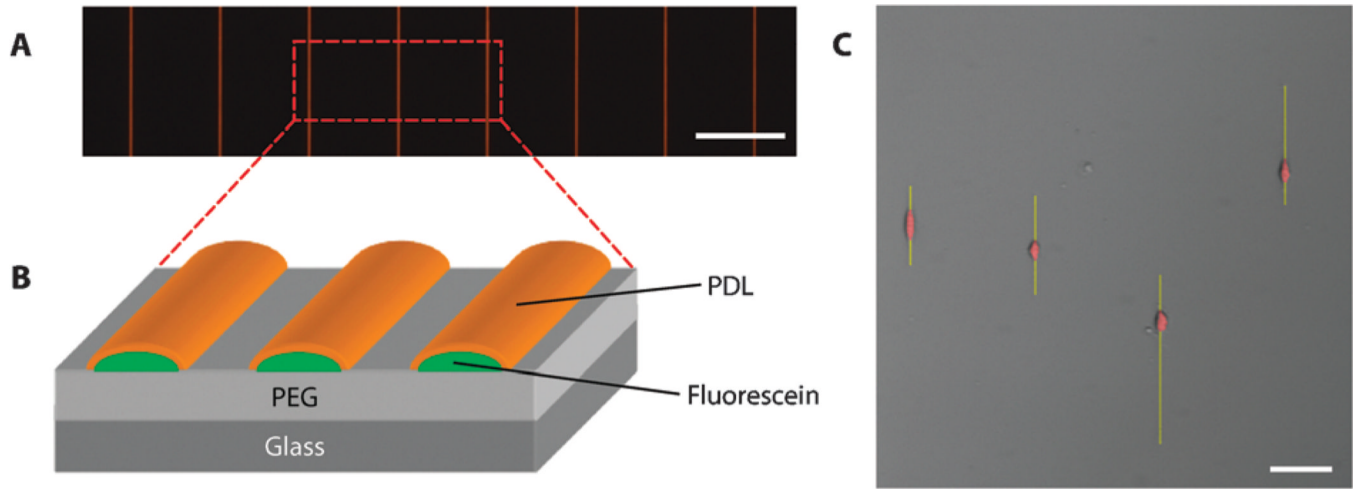

Fig. 1.

Hippocampal neuron culture on laser-patterned substrates. (A) Fluorescent image showing long uniform lines of polylysine, which were used as a substrate for the growth of hippocampal neurons (scale bar: 100 μm). (B) The lines were created by patterning fluorescein onto a PEG monolayer using a femtosecond laser and then incubating in a solution containing PDL, which selectively bound to the fluorescein. (C) False-colored phase-contrast image showing that hippocampal neurons adhered exclusively to the PDL patterns spaced 100 μm apart. The geometry of the lines prevented the neurons from growing more than one neurite in each direction. The neurons were false-colored to enhance contrast (soma, red; neurites, yellow), but image brightness was conserved (scale bar: 50 μm).

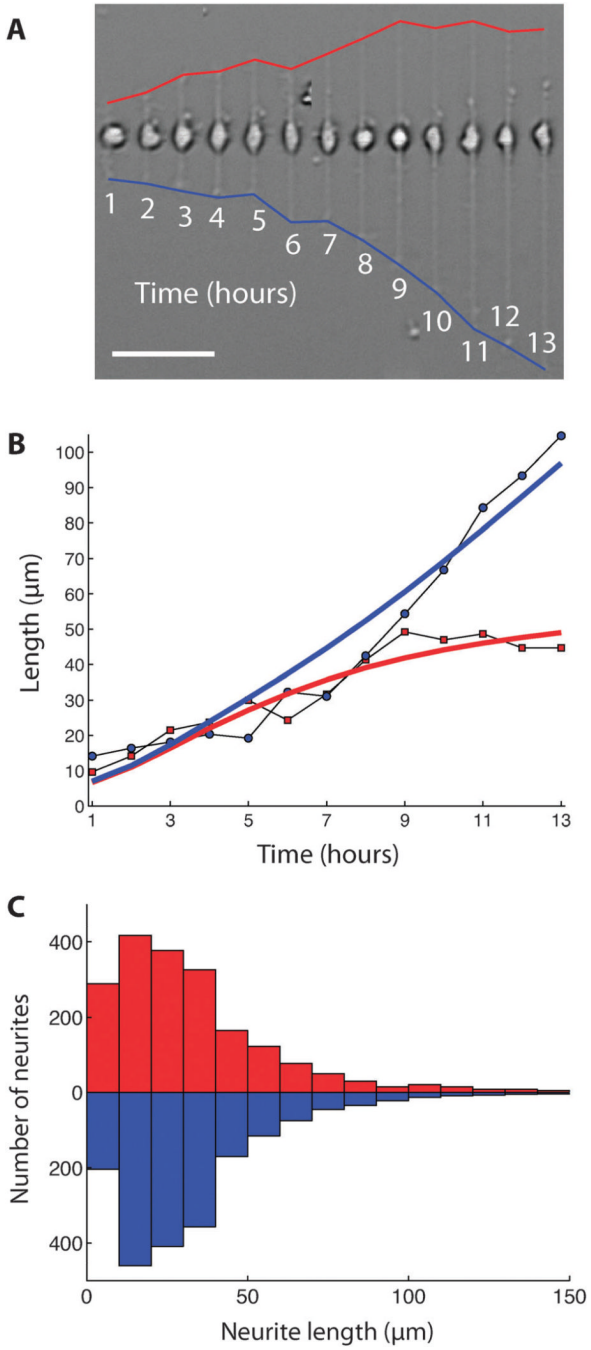

Fig. 2.

Neurite growth dynamics on laser-patterned substrates. (A) Time-lapse image of a neuron. The blue and red lines mark the extent of neurite growth over the course of 13 h (scale bar: 50 μm). (B) The red squares and blue circles mark the measured neurite lengths for the same neuron. The solid lines represent a best fit of the Samuels *et al.* model to the experimental data (t_{sc} = 4.3 h, L_{sc} = 46 μm, χ_1 = 3.2, χ_2 = 39, and χ_3 = 9.2). (C) Histogram of neurite lengths in one direction (red) *versus* the opposite direction (blue), where neurite lengths at all time points (*i.e.* from 1 to 18 h) are included.

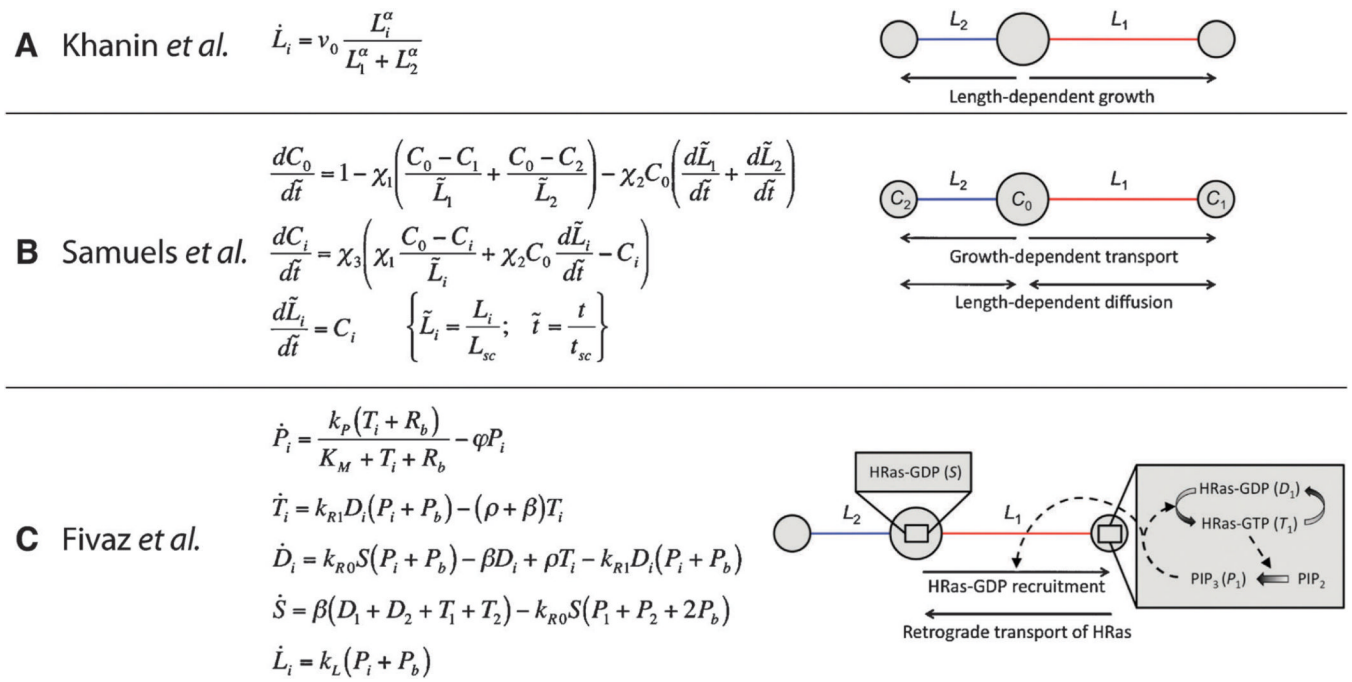

Fig. 3.

Leading models for neurite growth and competition. The subscript "*i*" is either 1 or 2, indicating the neurite. The larger and smaller circles indicate the soma *versus* neurite tips, respectively. (A) The Khanin *et al.* model involves the lengths of the two neurites (L_1, L_2), but no chemical concentrations. In this model, v_0 is the characteristic growth rate and α represents the strength of the competition between neurites. (B) The Samuels *et al.* model includes the concentrations (C_0, C_1, and C_2) of an unknown factor that is rate-limiting for neurite growth. The growth of a neurite is proportional to the concentration of the factor at that neurite's tip, and the factor undergoes both diffusion and length-dependent anterograde transport. Here, L_{sc} and t_{sc} are characteristic length and time scales, respectively, while χ_1, χ_2, and χ_3 are dimensionless constants. (C) The Fivaz *et al.* model describes the dynamics of multiple molecular species, including HRas, PI3K, PIP_2, and PIP_3. Phosphorylated HRas stimulates PI3K activation and PIP_3 production at the neurite tips. In turn, PIP_3 stimulates HRas phosphorylation in a positive feedback loop and the recruitment of additional HRas from the soma. In this model, k_P, k_{R0}, and k_{R1} are rate constants, φ and ρ are rates of protein degradation, β controls the rate of return of HRas to the soma, P_b and R_b are the respective baseline concentrations of PIP_3 and HRas, K_M relates to the concentration of HRas for half-maximal production of PIP_3, and k_L is the characteristic neurite growth rate. The Fivaz *et al.* model also incorporates stochastic vesicular transport, as discussed in the supporting information.

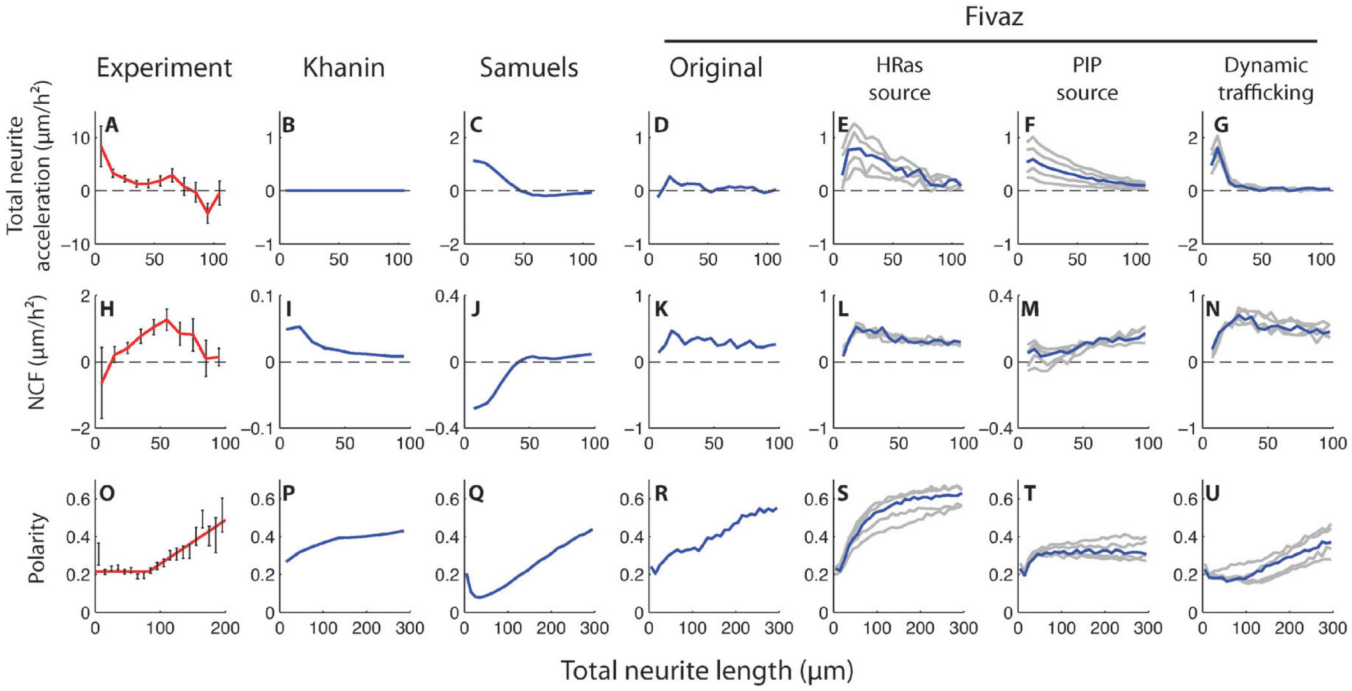

Fig. 4.

Neurite dynamics obtained from experimental measurements and from simulations of various models. (A)-(G) Total neurite growth acceleration ($\ddot{L}_1+\ddot{L}_2$) *vs.* total neurite length (L_1+L_2). For the Khanin *et al.* and Samuels *et al.* models, 500 trials were averaged with randomized initial conditions. For variations of the Fivaz *et al.* model, 200 trials were averaged, also with randomized initial conditions and stochastic vesicular transport. (H)-(N) Neurite competition factor (NCF) *vs.* total neurite length. Again, 500 trials were averaged for the Khanin *et al.* and Samuels *et al.* models, while 200 trials were averaged for the Fivaz *et al.* models. (O)-(U) Neuronal polarity *vs.* total neurite length. Neuronal polarity is defined as $|L_1-L_2|/(L_1+L_2)$. Error bars in (A), (H), and (O) represent the SEM. Three different variations of the Fivaz *et al.* model were analyzed: "HRas source" included a constant production term for HRas in the soma; "PIP source" included a constant production term for PIP_2, which was instantaneously transported to the neurite tips and phosphorylated, becoming PIP_3; "dynamic trafficking" involved an increasing, time-dependent rate of the transport of vesicles containing HRas from the soma to the neurite tips. These variations are further detailed in the supporting information. The tracings in (E), (L), and (S) represent HRas synthesis rates (*i.e.*, γ in the supporting information) between 0.004 and 0.020 (blue line is 0.012). The tracings in (F), (M), and (T) represent PIP_2 synthesis rates (κ in the supporting information) between 0.04 and 0.20 (blue line is 0.12). The tracings in (G), (N), and (U) represent time constants for vesicle trafficking (τ in the supporting information) between 4 and 12 h (blue line is 8 h).

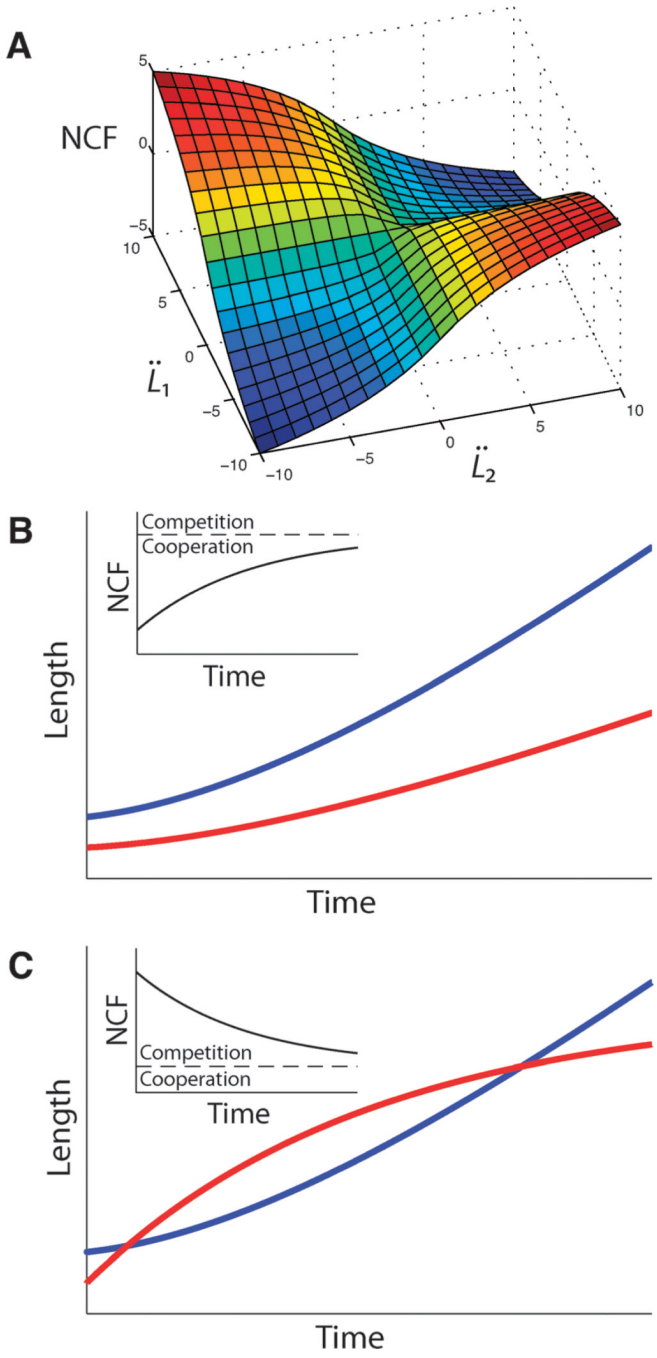

Fig. 5.

Illustration of neurite competition and cooperation in growing neurite pairs. Neurite lengths are plotted as a function of time. (A) Plot of the accelerations in the growth rates of two competing neurites *vs.* the neurite competition factor (NCF). Red indicates strong competition (positive NCF), while blue indicates strong cooperation (negative NCF). (B,C) Simulated examples of cooperating and competing neurites. (**Insets**) NCF as a function of time. The dashed lines indicate zero competition/cooperation. (B) Both neurites (red and blue) have increasing growth rates, yielding a negative (NCF), *i.e.*, cooperation. (C) While one neurite's growth rate is increasing (blue), the other neurite's growth rate is decreasing

(red), yielding a positive NCF, *i.e.*, competition. The NCF in both (B) and (C) approaches zero over time as the neurite growth rates approach constant values.

Table 1

Predictions of different models *vs*. experimental outcomes. The Khanin *et al*. model does not allow accelerative neurite growth, results in neurite competition that monotonically decreases with neurite length, and does not produce a phase transition in neuronal polarity. The Samuels *et al*. model predicts accelerative neurite growth and results in cooperation rather than competition between short neurites. The Fivaz *et al*. model does not predict accelerative growth, weak competition between long neurites, or a phase transition in neuronal polarity. Three simple modifications of the model ("HRas source," "PIP source," and "dynamic trafficking") recapitulate accelerative growth, but do not predict the weaker competition between long neurites. Of these modifications, only "dynamic trafficking" results in an apparent phase transition in neuronal polarity

	Experiment	**Khanin *et al.***	**Samuels *et al.***	**Fivaz *et al.***	**HRas source**	**PIP source**	**Dynamic trafficking**
Accelerative growth of short neurites	✓	✗	✓	✗	✓	✓	✓
Weak competition between short neurites	✓	✗	✗	✓	✓	✓	✓
Strong competition between intermediate neurites	✓	✗	✗	✓	✓	✗	✓
Weak competition between long neurites	✓	✓	✓	✗	✗	✗	✗
Phase transition in neuronal polarity	✓	✗	✓	✗	✗	✗	✓